International Journal of High-Rise Buildings
September 2013, Vol 2, No 3, 229-244

International Journal of
High-Rise Buildings
www.ctbuh-korea.org/ijhrb/index.php

Peak Pressures Acting on Tall Buildings with Various Configurations

Eswara Kumar Bandi[1†], Hideyuki Tanaka[2], Yong Chul Kim[3], Kazuo Ohtake[2], Akihito Yoshida[1], and Yukio Tamura[1]

[1]*Wind Engineering Research Center, Tokyo Polytechnic University, Kanagawa 243-0297, Japan*
[2]*Environmental Engineering Department, Takenaka Research & Development Institute, Takenaka Corporation, Chiba 270-1395, Japan*
[3]*School of Architecture, Seoul National University of Science and Technology, Seoul 139-743, Korea*

Abstract

Twenty six pressure models of high rise buildings with various cross-sections including twisted models were tested in a boundary layer wind tunnel. The cross-sections were triangular, square, pentagon, hexagon, octagon, dodecagon, circular, and clover. This study investigates variations in peak pressures, and effects of various cross-sections and twist angles on peak pressures. To study the effects of various configurations and twist angles on peak pressures in detail, maximum positive and minimum negative peak pressures at each measurement point of the building for all wind directions are presented and discussed. The results show that peak pressures greatly depend on building cross-section and twist angle.

Keywords: High-rise buildings, Peak pressures, Corner modifications, Twist angle, Helical models, Polygonal shapes

1. Introduction

Tall buildings are very common now in urban areas all over the world. It is very important to study peak suctions on roofs and walls, because they cause frequent damage under strong wind conditions. In turbulent flows, peak suctions occasionally occur near the corners of walls and roofs (Melbourne, 1993). Saathoff et al. (1989) investigated the occurrence of large negative peak pressures near the leading edges of sharp-edged bluff bodies. Stathopoulos et al. (1991) studied local pressure coefficients on multi-span gabled (folded) roofs of low buildings. Surry et al. (1995) studied the peak suctions developed on building models and their relationship with building shapes. Many researchers investigated the effect of corner modifications on peak pressure coefficients, Jamieson et al. (1992); Kazuo (2000); Junji et al. (1992). Kawai et al. (2002) investigated the effects of edge modifications on peak suctions. Kim et al. (2010) also studied wind pressures on Square, Taper and Setback models to investigate the aerodynamic force reduction. Hirotoshi et al. (1997) studied the characteristics of peak wind pressures acting on tall building model.

†Corresponding author: Eswara Kumar Bandi
Tel: +81-46-242-9547; Fax: +81-46-242-9547
E-mail: bekreddybandi@yahoo.com

2. Experimental Setup

Wind tunnel tests were conducted in a boundary layer wind tunnel at the Wind Engineering Research Center, Tokyo Polytechnic University, Japan. The wind tunnel test section was 19 m long and had a cross-section 2.2 m wide by 1.8 m high. Models 0.4 m high were used. The high rise building models examined in this study are classified into 5 categories: such as Polygonal (Triangular, Square, Pentagon, Hexagon, Octagon, Dodecagon and Circular), Tapered, Helical (Polygonal helical: Tri-180°Hel, Sq-180° Hel, Penta-180°Hel, Hexa-180°Hel, Octa-180°Hel and Dodeca-180°Hel models), corner modification and combination, as shown in Table 1(a)-(e). The combination models shown in Table 1(e) have the combined configurations of the primary configurations shown in Table 1(a)-(d). All the models had the same volume, and they were tested to identify their aerodynamic characteristics. The colored surfaces shown in Table 2 are those shown as straight surfaces for the distribution of largest negative peak and largest positive peak pressures. There were about 21 measurement points for the Triangular models and 24 measurement points for the Tri-Corner cut and Clover models on each level on three surfaces as shown in the following Table 3, and the measurement points were instrumented at 10 levels giving about 210 measurement points for the Triangular models and about 240 measurement points for the Tri-Corner cut and Clover models. All the pressure models discussed in this paper have the measurement points at 10

Table 1. Configurations of the models

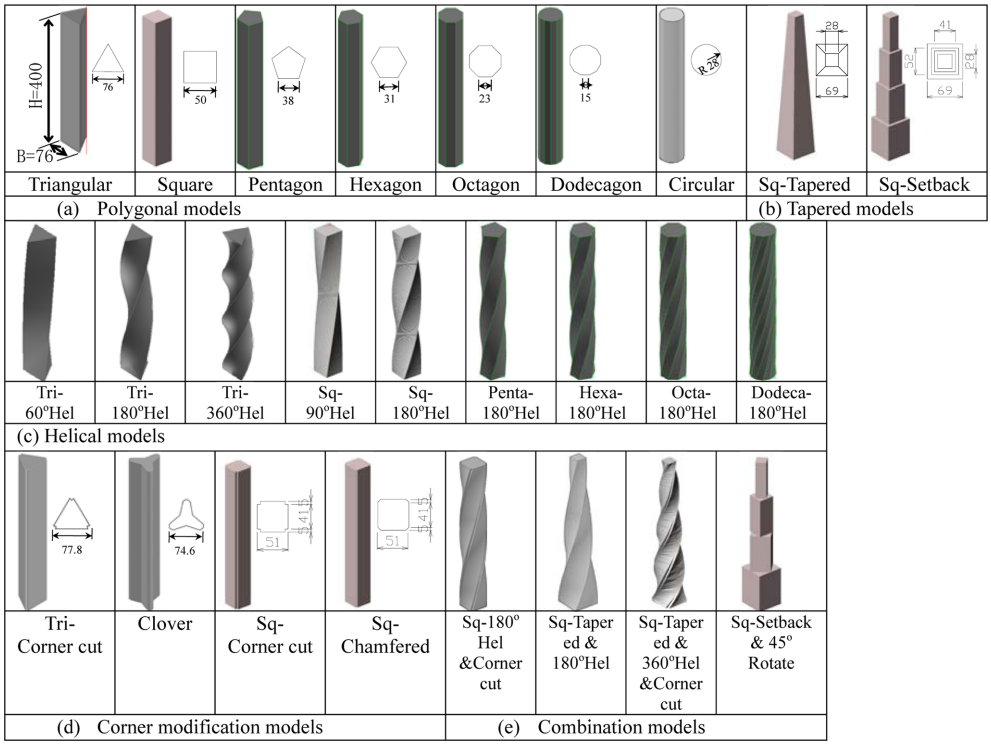
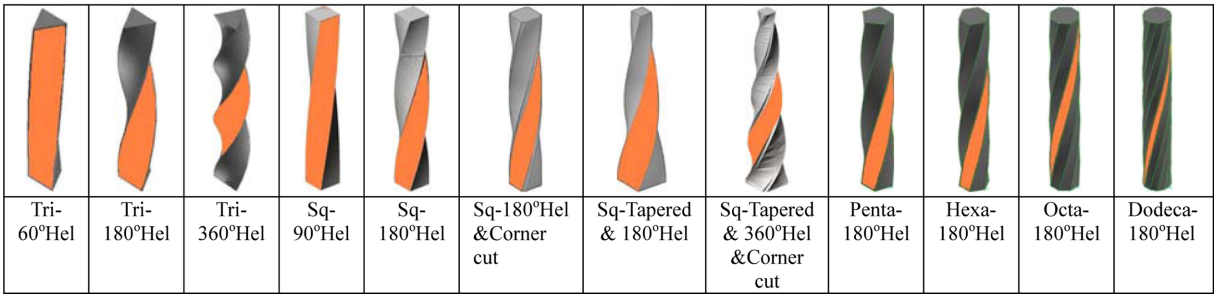


Table 2. The colored surfaces for the distribution of peak pressures



levels and the height of each level for all the models is same. The total number of measurement points for each model varies from 184 to 250.

The profiles of mean wind speed and turbulence intensity are shown in Figure 1. The experiments were conducted for an urban (power-law exponent, $\alpha = 0.27$) flow, with changing wind directions. Using a hot wire anemometer, the wind speed at the model height was measured at around 12 m/s for urban flow conditions.

A length scale of 1/1000 and a time scale of 1/167 were assumed. All the pressures were measured simultaneously with a sampling frequency of 781 Hz, and a low-pass filter with a cut-off frequency of 300-Hz was cascaded in each data acquisition channel to eliminate aliasing effects. For the negative peak wind pressure coefficients, a moving average with points corresponding to 0.5 sec in full time scale was applied, and 9 samples corresponding to 10 minutes in full time scale were used. The Reynolds number was about 9.6×10^4. Blockage corrections were not applied to the experimental results. There is a difference in peak pressure coefficients of around 10 to 13% for Square model accompanied by corner modification & tapered models, and the same Square model accompanied by polygon models due to the experiments being conducted in different wind tunnels. The trend of increasing or decreasing peak pressure coefficients mentioned in the text is based on their magnitudes only.

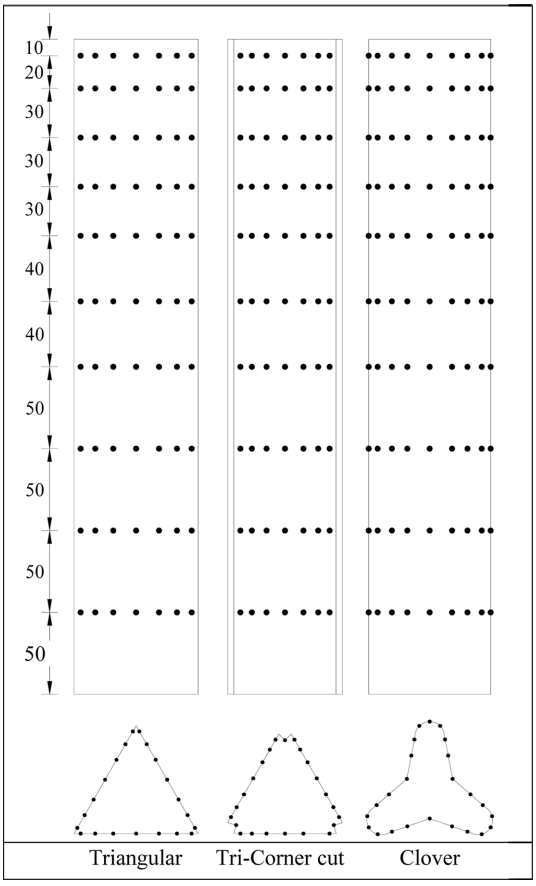
3. Results and Discussions

Wind pressure coefficients are calculated from the pressure time series of each pressure tap, $C_p(t)$ using Eq. (1).

$$C_p(t) = \frac{p(t)}{0.5\rho(U_H)^2} \tag{1}$$

$$\check{C}_p = \min(C_p(t), \theta)$$

Table 3. Arrangement of pressure taps and coordinate system (Unit: mm)



$$\hat{C}_p = \max(C_p(t), \theta)$$

Where $p(t)$ is the time series of wind pressure; ρ the air density (1.25 kg/m^3); U_H the mean wind speed at the top of the building models; θ is wind direction; $\check{C}_p$ the largest negative peak pressure coefficient among all tap locations at each wind direction; $\hat{C}_p$ the largest positive peak pressure coefficient among all tap locations at each wind direction;

3.1. Effect of corner modifications on peak pressures

This section, considers corner modification models of Triangular and Square cross-sections. The models considered were Triangular, Tri-Corner cut, Clover, Square, Sq-Corner cut and Sq-Chamfered models, as shown in Table 1(d). The largest negative and positive peak pressures were selected for all wind directions.

3.1.1. Largest positive peak pressure coefficients of all wind directions ($\hat{C}_p(i)$)

Figure 2 shows the distribution of largest positive peak pressure coefficients of the models for all wind directions, ($\hat{C}_p(i)$). The $\hat{C}_p(i)$ distributions vary smoothly for all models. The maximum $\hat{C}_p(i)$ values occur at upper levels for all models. The $\hat{C}_p(i)$ distribution varies smoothly from lower to the higher values from corner regions to the center of the surfaces for the Tri-Corner cut and Clover models whereas $\hat{C}_p(i)$ is almost constant for the Square models. The absolute largest positive peak pressure coefficients of all wind directions and tap locations were Triangular: 1.79, Tri-Corner cut: 1.64, Clover: 1.62, Square: 1.44, Sq-Corner cut: 1.43, and Sq-Chamfer: 1.45.

3.1.2. Largest negative peak pressure coefficients of all wind directions ($\check{C}_p(i)$)

Figure 3 show the distribution of largest negative peak pressure coefficients of the models for all wind directions, ($\check{C}_p(i)$). The $\check{C}_p(i)$ distributions vary smoothly from corner regions to the center of the surfaces for all models. The largest peak suctions occur close to the corner regions for all the models, and it occurs between 0.4H-0.78H for the Tri-Corner cut, Clover, Square, Sq-Corner cut and Sq-Chamfered models, whereas for Triangular model it occurs at 0.98H. The absolute largest negative peak pressure coefficients of all wind directions and tap locations were Triangular: 3.75, Tri-Corner cut: 3.12, Clover: 3.13, Square: 2.68, Sq-Corner cut: 3.20, and Sq-Chamfer: 2.75.

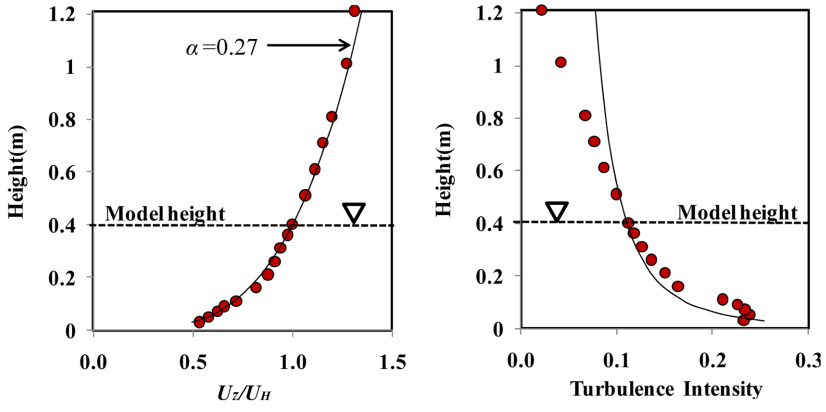


Figure 1. Profile of mean wind speed and turbulence intensity.

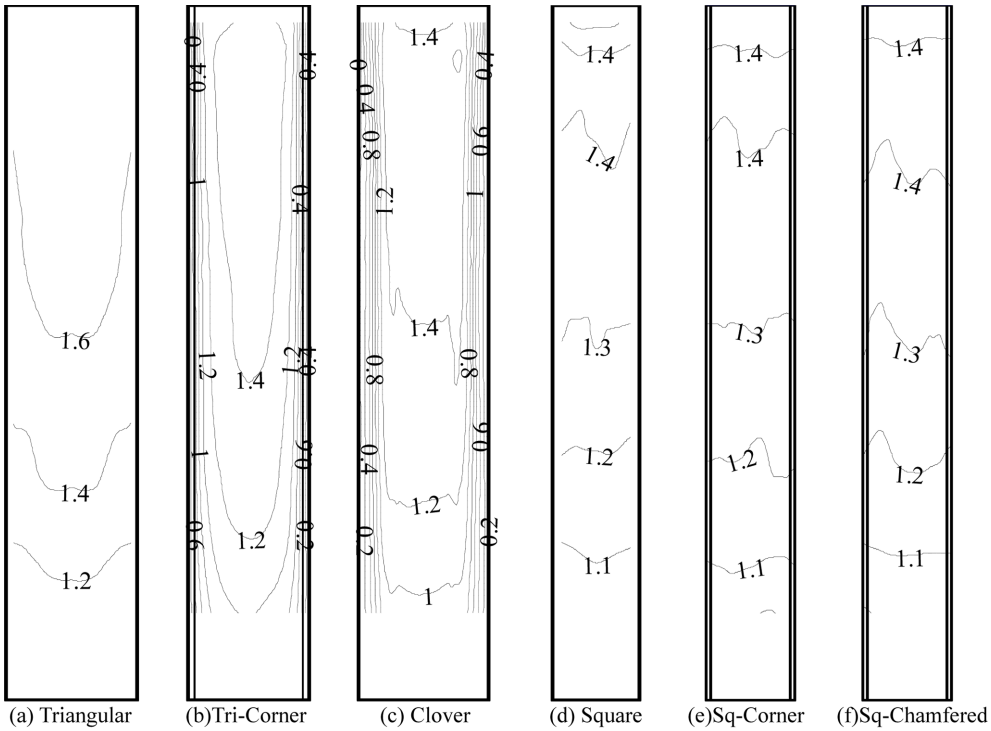


Figure 2. Largest positive peak pressure coefficients for all wind directions for Square and Triangular models.

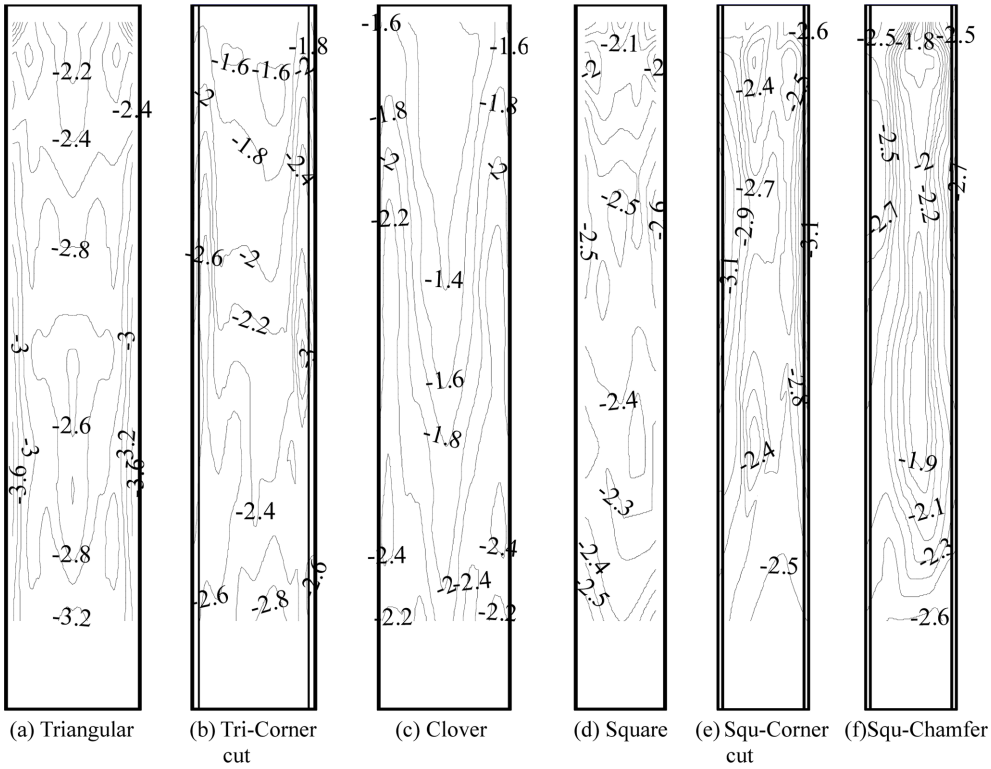


Figure 3. Largest negative peak pressure coefficients for all wind directions for Square and Triangular models.

3.1.3. Effect of corner modifications

The effect of corner modifications on largest negative peak pressure coefficients at $0.85H$ ($\check{C}_{P,\,0.85H}$) has been investigated for all wind directions for the Triangular, Tri-Corner cut, Clover, Square, Sq-Corner cut and Sq-Chamfered models. Points a, b, c, d and e in Figures 4 and 5 are

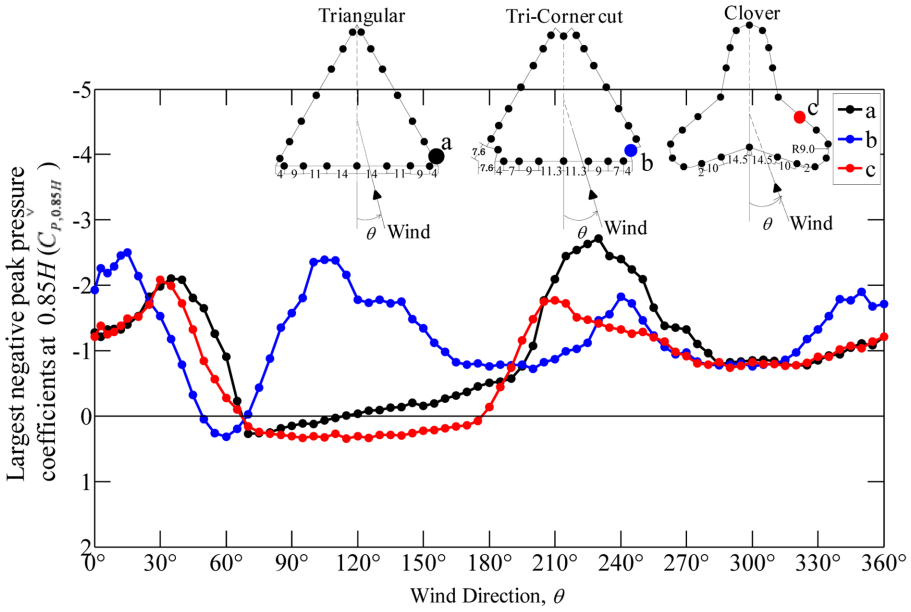


Figure 4. Effect of corner modification on largest negative peak pressure coefficients at *0.85H* for corner modification models of Triangular cross-section.

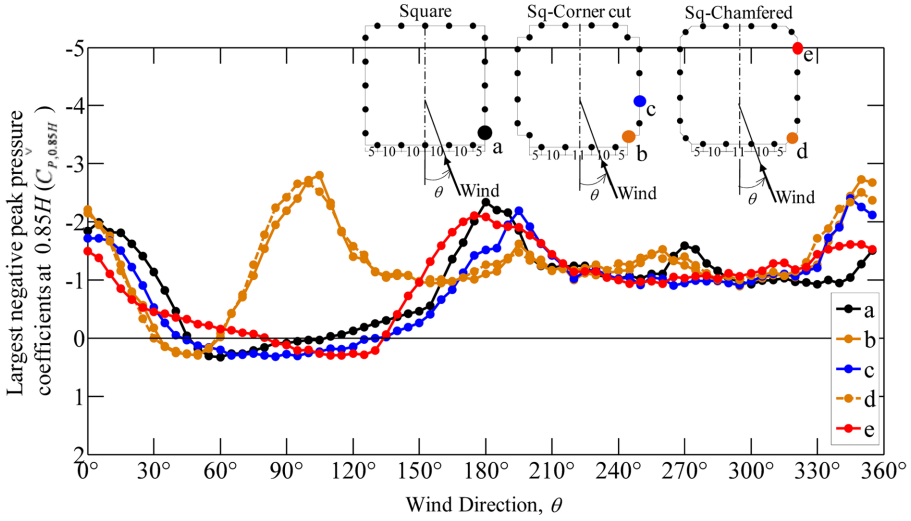


Figure 5. Effect of corner modification on largest negative peak pressure coefficients at *0.85H* for corner modification models of Square cross-section.

where the maximum $\breve{C}_{P,0.85H}$ occurred on the side surface. Figures 4 and 5 show the variation of $\breve{C}_{P,0.85H}$ with wind direction of the above mentioned points. Figure 4, show clearly that $\breve{C}_{P,0.85H}$ reduces for the Tri-Corner cut for most of wind directions except 0° to 25°, 70° to 185° and 320° to 360°, whereas for the Clover model $\breve{C}_{P,0.85H}$ reduces for all wind directions. The $\breve{C}_{P,0.85H}$ values for the Tri-Corner cut model are less than the maximum value for the Triangular model. The $\breve{C}_{P,0.85H}$ values are equal for the Triangular and Clover models at 30° wind direction where the flow is parallel to one of the surfaces of the Triangular model. The $\breve{C}_{P,0.85H}$ values are equal for the Triangular, Tri-Corner cut and Clover models at 25° and 285° to 315° wind directions. As shown in Figure 5, for the square cross-sections, the $\breve{C}_{P,0.85H}$ values reduce for the Sq-Corner cut and Sq-Chamfered models at point c and point e for most of wind directions. The location of the peak suctions shifts downstream on the surface for the Sq-Corner cut model compared with those of the Square, Triangular and Tri-Corner cut models, whereas the corner regions for the Sq-Corner cut and Sq-Chamfer models showed larger $\breve{C}_{P,0.85H}$ values when the flow was perpendicular (around 90° Wind direction) to the surface. The $\breve{C}_{P,0.85H}$ values followed the same trend and were almost the same for all wind directions except 60° to 160° for the Sq-Corner cut and Sq-Chamfered models at the specified locations. The $\breve{C}_{P,0.85H}$

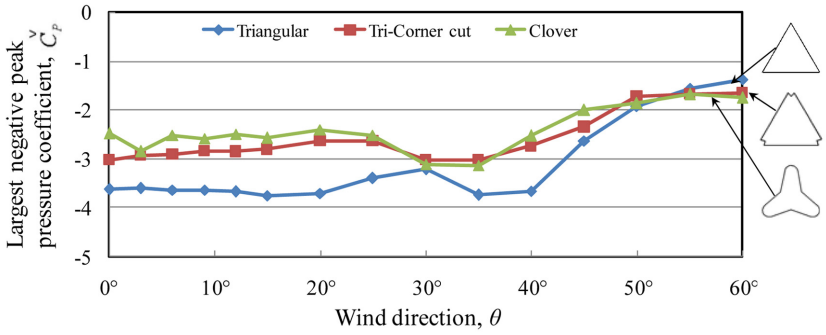


Figure 6. Variation of largest negative peak pressure coefficients with wind direction (θ) for Triangular, Tri-Corner cut and Clover models.

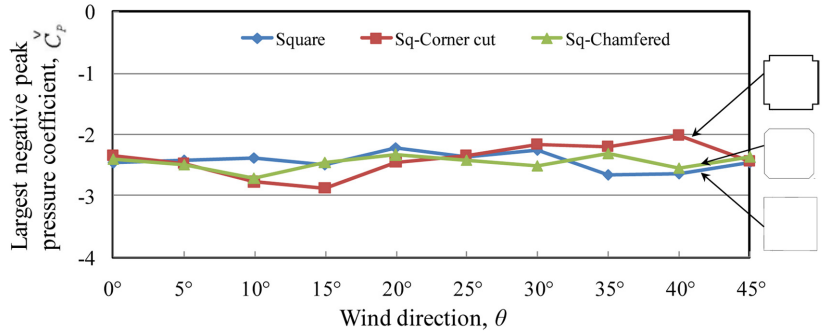


Figure 7. Variation of largest negative peak pressure coefficients with wind direction (θ) for Square, Sq-Corner cut and Sq-Chamfered models.

values followed the same trend between 60° and 185° for the Tri-Corner cut, Sq-Corner cut and Sq-Chamfered models.

3.1.4. Variation of largest negative peak pressure coefficients with wind direction (θ)

Figures 6 and 7 show the largest negative peak pressure coefficient among all tap locations at each wind direction, $\check{C}_P$. As shown in Figure 6, the largest and smallest $\check{C}_P$ occurred for the Triangular model. The smallest $\check{C}_P$ occurred for the Tri-Corner cut and Clover models when the corners of the models were perpendicular to the flow at wind directions close to 60°. Figure 7 shows the variation of $\check{C}_P$ for all wind directions for the Square, Sq-Corner cut and Sq-Chamfered models. Sq-Corner cut shows larger and smaller values than Square and Sq-Chamfered models. The $\check{C}_P$ values were the same for the Square, Sq-Corner cut and Sq-Chamfered when the flow was perpendicular to the surface ($\theta = 0°$) and corners ($\theta = 45°$). Also, the $\check{C}_P$ values were the same for the Tri-Corner cut and Clover models when the flow was perpendicular to the corner ($\theta = 60°$)

3.2. Effect of Taper on peak pressures

This section, considers the tapered models with square cross-sections and compares them with the Square model. The models are Square, Sq-Tapered and Sq-Setback shapes, as shown in Table 1(b).

3.2.1. Largest positive peak pressure coefficients of all wind directions ($\hat{C}_p(i)$)

Figure 8 shows the $\hat{C}_p(i)$ distribution for the Square, Sq-Tapered and Sq-Setback models. They vary smoothly for all models. For all models, the $\hat{C}_p(i)$ values increase with height. The $\hat{C}_p(i)$ distribution varies almost constantly for the Square and Sq-Taper models whereas for the Sq-Setback model, they are larger at the corner regions as in the case of $\hat{C}_p(i)$ values. The absolute largest positive peak pressure coefficients of all wind directions and tap locations were Sq-Taper: 1.43, and Sq-Setback: 1.44.

3.2.2. Largest negative local peak pressure coefficients of all wind directions ($\check{C}_P(i)$)

Figure 9 shows the $\check{C}_P(i)$ distribution for the models mentioned in 3.2.1. They vary smoothly for all models. The peak suctions occur close to the corner regions for the Square and Setback models whereas for the Taper model, the largest values occur at mid height of the center region and at $0.125H$ of the corner region. The largest suctions occur at the top corner regions of each step of the Sq-Setback model. The absolute largest negative peak pressure coefficients of all wind directions and tap locations were Sq-Taper: 2.34, and Sq-Setback: 3.05.

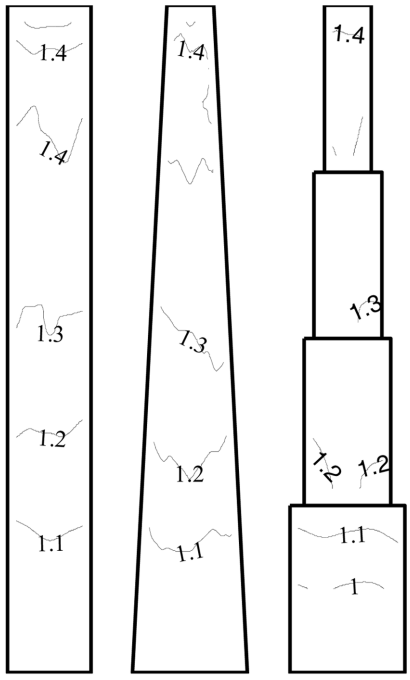


Figure 8. Largest positive peak pressure coefficients for all wind directions for Tapered models.

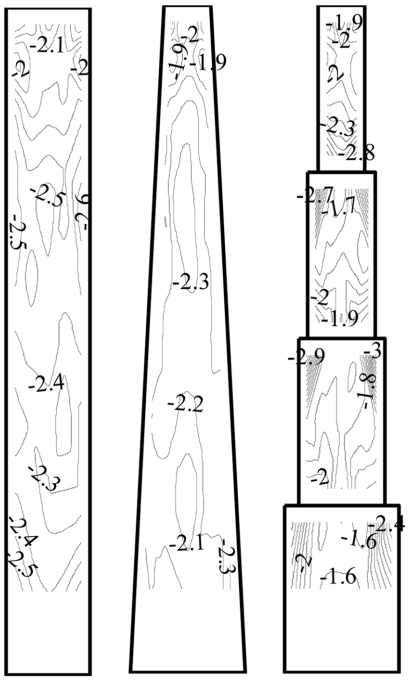


Figure 9. Largest negative peak pressure coefficients for all wind directions for Tapered models.

3.2.3. Variation of largest negative peak pressure coefficients with wind direction (θ)

Figure 10 shows the largest negative peak pressure coefficient among all tap locations at each wind direction, $\check{C}_P$. The largest and smallest $\check{C}_P$ values occur for the Sq-Setback model and the largest values occur for wind directions 0° to 10° when the flow is perpendicular to the surface. The variation between the largest and smallest values is larger than for the Square and Sq-Tapered models, whereas they vary between -1.88 and -2.34 for the Sq-Tapered model.

3.3. Effect of number of surfaces on peak pressures

This section, considers the polygonal models of Triangular, Square, Pentagon, Hexagon, Octagon, Dodecagon and Circular cross-sections, as shown in Table 1(a), and the effect of increasing number of surfaces on local peak pressures.

3.3.1. Largest positive peak pressure coefficients of all wind directions ($\hat{C}_p(i)$)

Figure 11 shows the $\hat{C}_p(i)$ distributions for all the polygonal models with increasing of number of surfaces. They vary smoothly for all models. $\hat{C}_p(i)$ values occur at heights from $0.85H$ to $0.925H$ for all models, whereas for the Pentagon model a slightly higher $\hat{C}_p(i)$ also occurs even at the acute bottom corner ($0.125H$). $\hat{C}_p(i)$ values decrease as the width of the surface decreases for the Triangular, Square, Pentagon and Hexagon models, as seen in the Figure 11. The absolute largest positive peak pressure coefficients of all wind directions and tap locations were Pentagon: 1.64, Hexagon: 1.62, Octagon: 1.68, Dodecagon: 1.66, and Circular: 1.53.

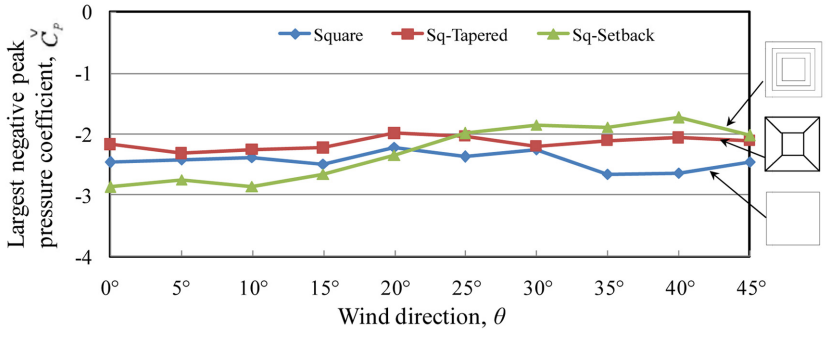


Figure 10. Variation of largest negative peak pressure coefficients with wind direction (θ) for Tapered models.

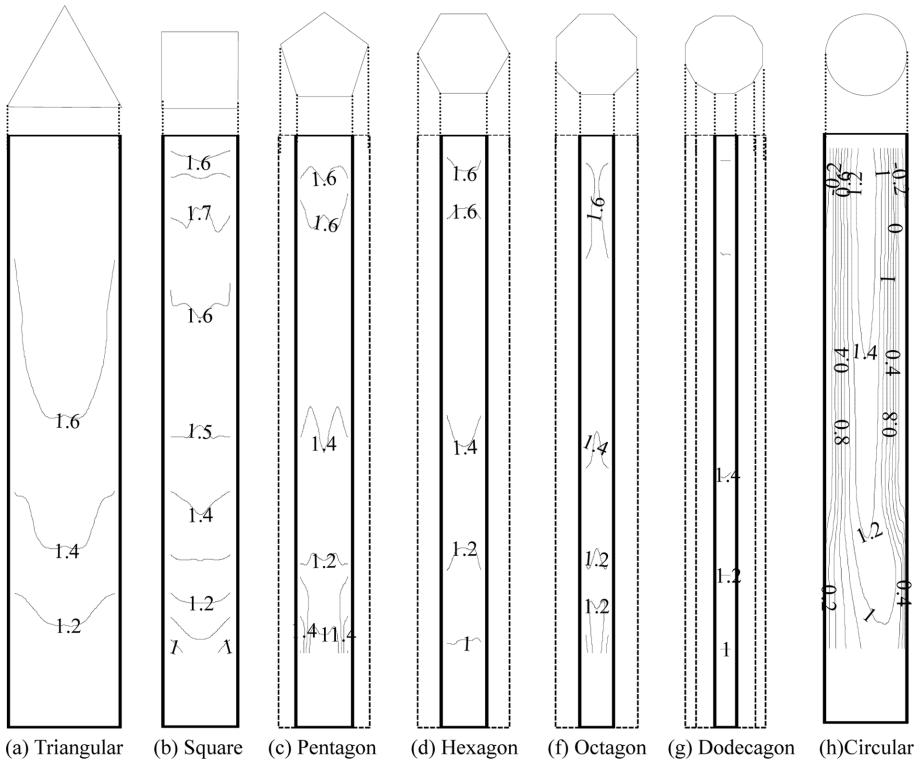


Figure 11. Largest positive peak pressure coefficients for all wind directions for Polygon models.

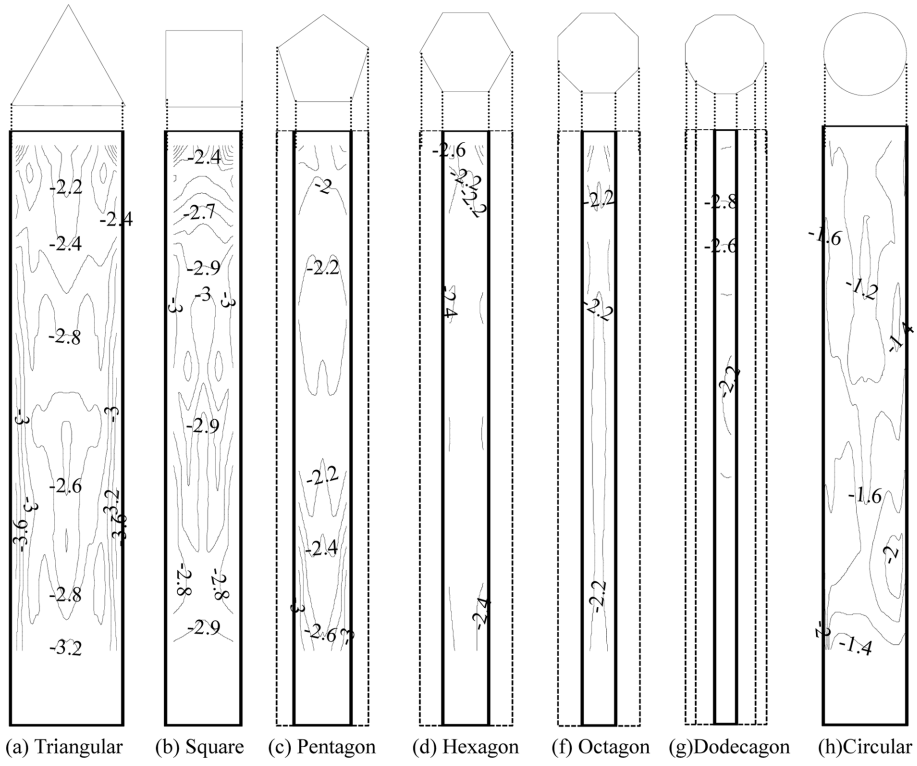


Figure 12. Largest negative peak pressure coefficients for all wind directions for Polygon models.

3.3.2. Largest negative peak pressure coefficients of all wind directions ($\check{C}_P(i)$)

Figure 12 shows the $\check{C}_P(i)$ distributions for all the polygonal models with increase in number of surfaces. They vary smoothly for all models. The largest peak suctions occur close to the corner regions for all models at various

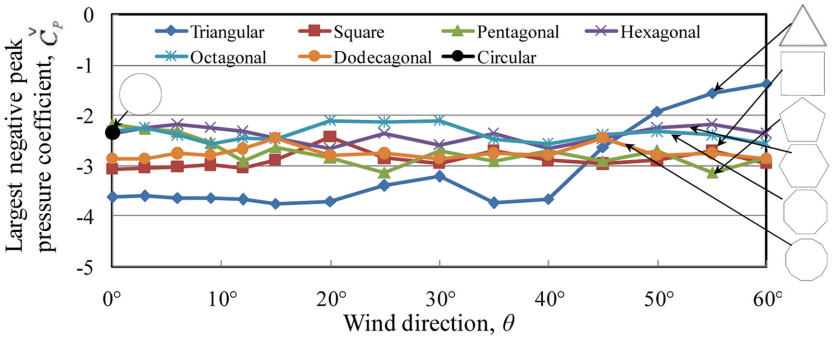


Figure 13. Variation of largest negative peak pressure coefficients with wind direction (θ) for Polygonal models.

heights. The peak suctions occur at 0.6H, 0.78H, 0.125H, 0.98H, 0.98H, 0.98H and 0.125H for the Triangular, Square, Pentagon, Hexagon, Octagon, Dodecagon and Circular models. For the Pentagon model, the peak suctions occurs at the acute bottom corner whereas for the Hexagon model, they occur at the top and at the acute bottom corners as well. The absolute largest negative peak pressure coefficients of all wind directions and tap locations were Pentagon: 3.13, Hexagon: 2.65, Octagon: 2.56, Dodecagon: 2.85, and Circular: 2.33.

3.3.3. Variation of largest negative peak pressure coefficients with wind direction (θ)

Figure 13 shows the largest negative peak pressure coefficient among all tap locations at each wind direction, $\check{C}_P$ for all the polygonal models. As shown in the Figure 13, the largest and smallest $\check{C}_P$ values occur for the Triangular model. When the flow is perpendicular to one of the surfaces (wind direction, $\theta = 0^o$), the $\check{C}_P$ value is maximum for the Triangular model and it reduces when the number of surfaces increases, but the largest $\check{C}_P$ is around -2.2 for the Pentagon, Hexagon, Octagon and Circular models.

3.4. Effects of twisting angle of helical models on peak pressures

This section, considers the helical models with various twisting angles, as shown in Table 1(c).

3.4.1. Largest positive peak pressure coefficients of all wind directions ($\hat{C}_p(i)$)

Figures 14, 16 and 18 show the $\hat{C}_p(i)$ distributions for the helical models of Triangular cross-section (Tri-60°Hel, Tri-180°Hel, and Tri-360°Hel), Square cross-section (Sq-90°Hel and Sq-180°Hel), and polygonal models (Tri-180° Hel, Sq-180°Hel, Penta-180°Hel, Hexa-180°Hel, Octa-180° Hel, and Dodeca-180°Hel). They vary smoothly for the Triangular and Square models as we can seen from Figure 10, but for the Helical models they also vary smoothly and increase towards upper levels. The $\hat{C}_p(i)$ values are higher for the helical models of Triangular cross-sections than for

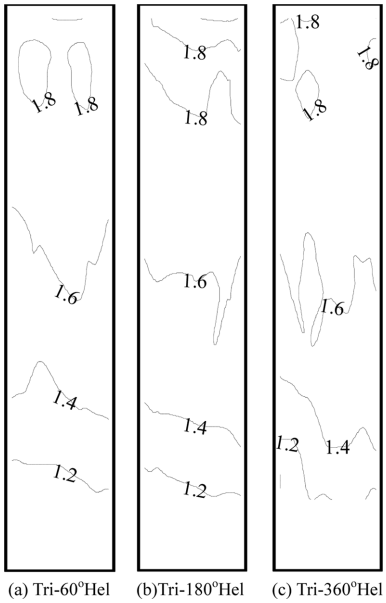


Figure 14. Largest positive peak pressure coefficients for all wind directions for Triangular helical models.

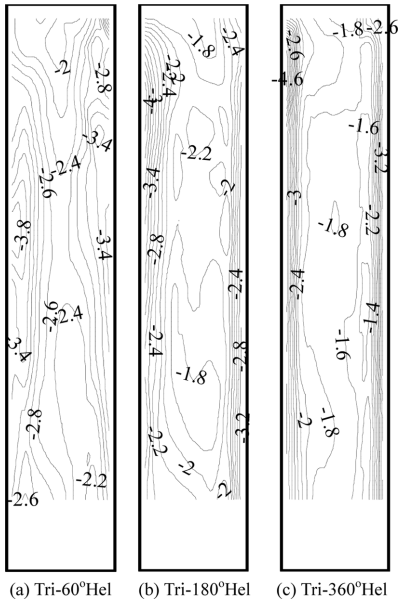


Figure 15. Largest negative peak pressure coefficients for all wind directions for Triangular helical models.

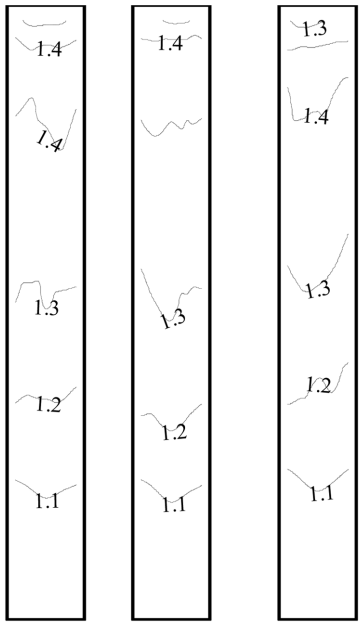


Figure 16. Largest positive peak pressure coefficients for all wind directions for Square helical models.

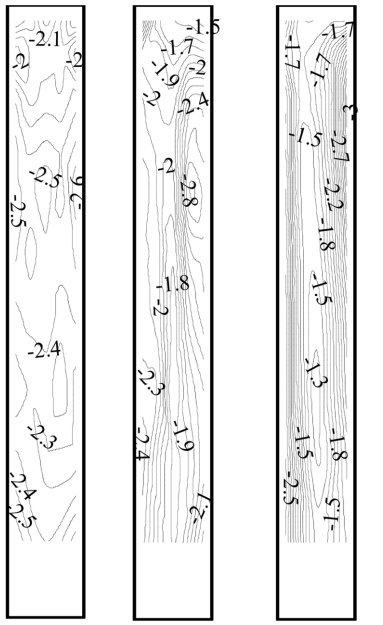


Figure 17. Largest negative peak pressure coefficients for all wind directions for Square helical models.

the helical models of Square cross-sections. The maximum $\hat{C}_P(i)$ values occur at $0.125H$ for Penta-180°Hel as in the case of the straight Pentagon model.

3.4.2. Largest negative peak pressure coefficients of all wind directions ($\check{C}_P(i)$)

$\check{C}_P(i)$ distributions were discussed for the helical models in 3.4.1. Figures 15, 17, and 19 show the $\check{C}_P(i)$ distributions for all helical models. They vary smoothly for the Triangular and Square models as can be seen in Figure 12, but for the helical models they vary widely, showing larger differences between the corner regions and on the surfaces. $\check{C}_P(i)$ increases as the twisting angle of the Helical model increases for both Triangular and Square cross-sectional models. Occurrence height of peak suctions also increases with twisting angle of the Helical

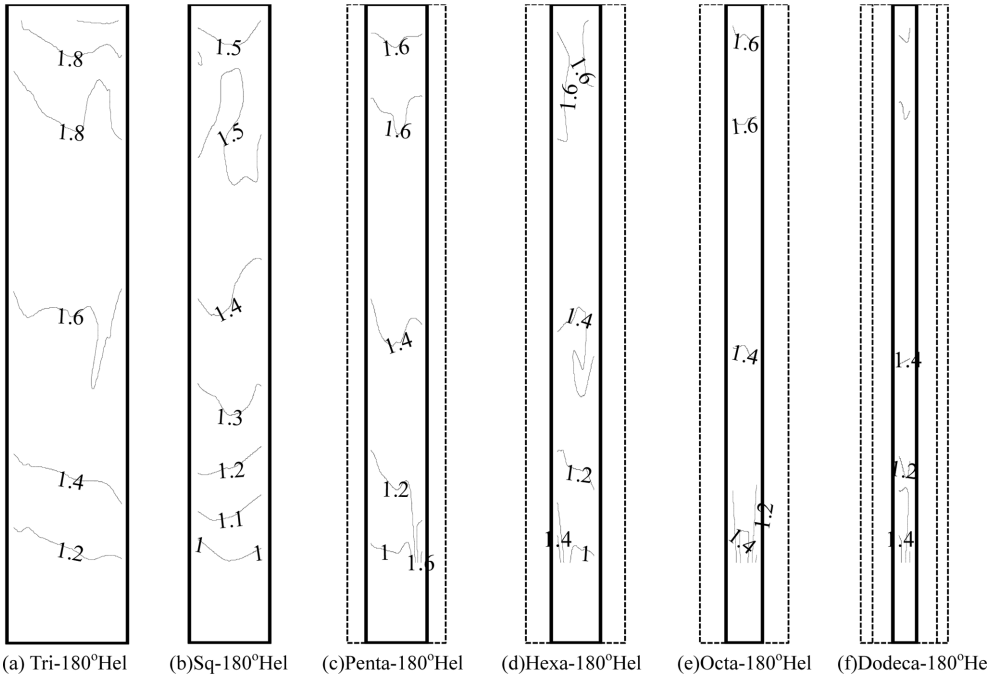


Figure 18. Largest positive peak pressure coefficients for all wind directions for polygonal helical models.

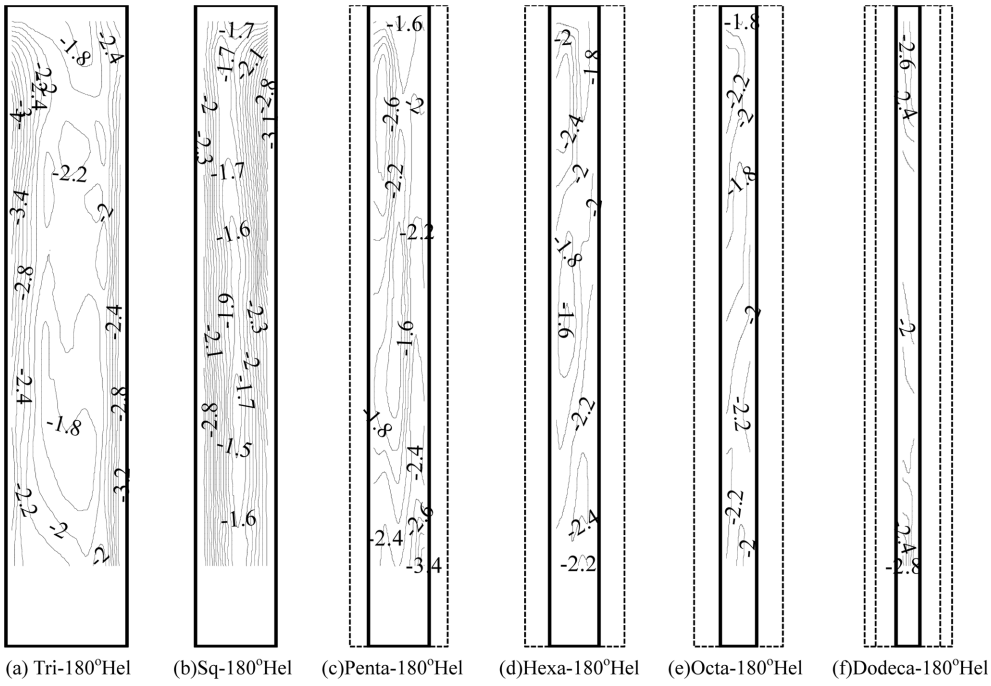


Figure 19. Largest negative peak pressure coefficients for all wind directions for polygonal helical models.

models. The maximum $\check{C}_P(i)$ occur at heights 0.85H - 0.925H for all the helical models of polygonal shapes, whereas it occur at 0.125H for the Penta-180°Hel model. The variation of $\check{C}_P(i)$ between upper and lower levels of the models reduces as the number of surfaces increases for the 180°Helical polygon models.

3.4.3. Variation of largest negative peak pressure coefficients with wind direction (θ)

Figures 20~22 show the largest negative peak pressure coefficient among all tap locations at each wind direction, $\check{C}_P$ for all the helical models. At 0° wind direction the $\check{C}_P$ values are higher for the Tri-360°Helicl model and decrease as twisting angle decreases, whereas for the Square cross-section helical models, it is the same at 0° wind direction, as can be seen in Figure 21. The variation of $\check{C}_P$ with wind direction is high for the helical models of Triangular cross-sections and the variation is low for the helical models of Square cross-sections, whereas the variation of $\check{C}_P$ with wind direction is low for the Octa-180°Hel model compared with all polygonal helical models.

3.5. Combined effect of corner modification and helical on local peak pressures

This section, considers the combination models shown in Table 1(e). The models are Sq-180°Hel & Corner cut, Sq-Tapered & 180°Hel, Sq-Tapered & 360°Hel &Corner cut, and Sq-Setback & 45° Rotate.

3.5.1. Largest positive and negative local peak pressure coefficients of all wind directions ($\hat{C}_p(i)$ and $\check{C}_P(i)$)

Figure 23 shows the $\hat{C}_p(i)$ distribution for the Sq-180° Hel &Corner cut, Sq-Tapered & 180°Hel, Sq-Tapered & 360°Hel &Corner cut, and Sq-Setback & 45° Rotate models. The $\hat{C}_p(i)$ values vary smoothly for all models. The absolute largest positive peak pressure coefficients of all wind directions and tap locations occur at the model height of the model for all models. They are Sq-180°Hel

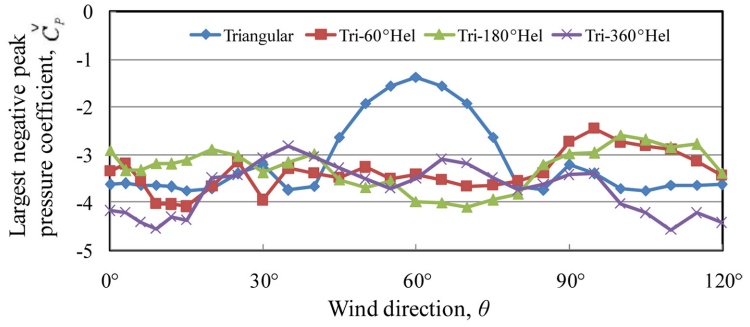


Figure 20. Variation of largest negative peak pressure coefficients with wind direction (θ) for Triangular helical models.

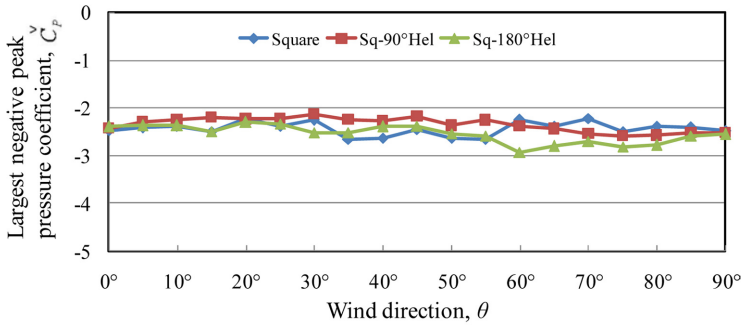


Figure 21. Variation of largest negative peak pressure coefficients with wind direction (θ) for Square helical models.

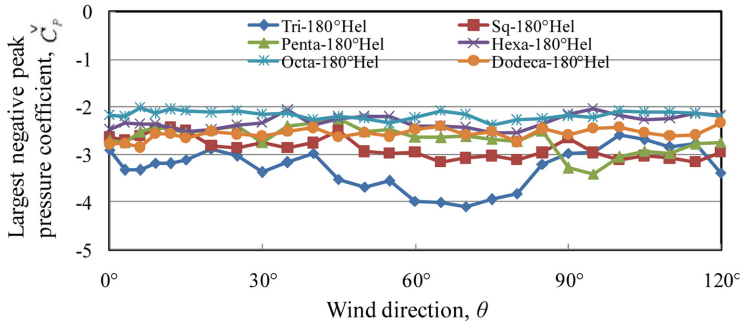


Figure 22. Variation of largest negative peak pressure coefficients with wind direction (θ) for Polygoanl helical models.

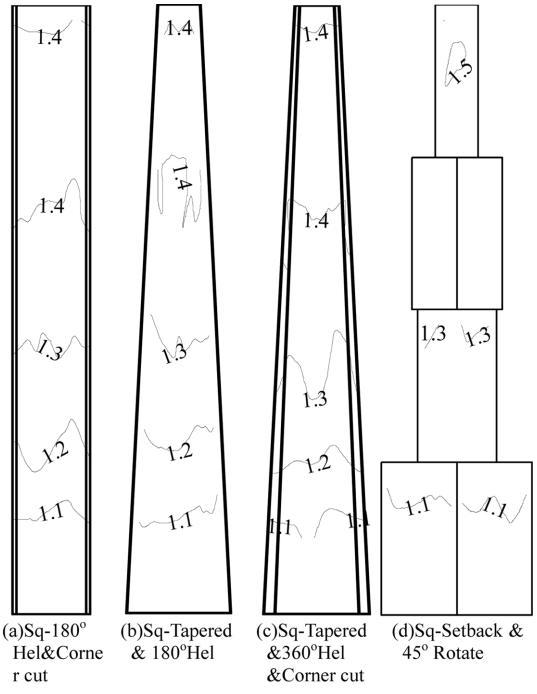


Figure 23. Largest positive peak pressure coefficients for all wind directions for Combination models.

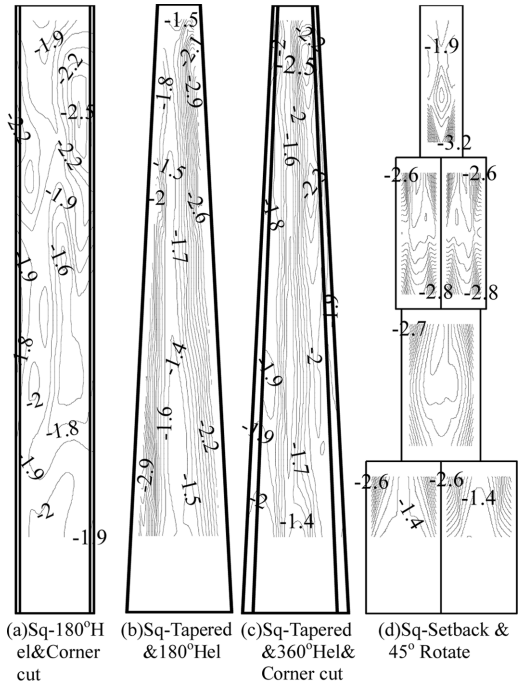


Figure 24. Largest negative peak pressure coefficients for all wind directions for Combination models.

& Corner cut: 1.47, Sq-Tapered & 180°Hel: 1.45, Sq-Tapered & 360°Hel&Corner cut: 1.48, and Sq-Setback & 45°Rotate: 1.51. The $\check{C}_P(i)$ distributions vary widely for all the models shown in Figure 24. Peak suctions occur above 0.5*H* for the corner-cut (Sq-180°Hel & Corner cut, and Sq-Tapered & 360°Hel & Corner cut) models, whereas for the Sq-Tapered & 180°Hel and Sq-Setback & 45° Rotate models, peak suctions occur even at 0.125*H*. For the Sq-Set-

back & 45°Rotate model, the peak suction occurs at the corners of all the set-backing steps. The absolute largest negative peak pressure coefficients of all wind directions and tap locations were Sq-180°Hel & Corner cut: 2.49, Sq-Tapered & 180°Hel: 2.94, Sq-Tapered & 360°Hel & Corner cut: 2.51, and Sq-Setback & 45° Rotate: 3.2.

3.5.2. Variation of largest negative peak pressure coefficients with wind direction (θ)

Figures 25~28 show the largest negative peak pressure coefficient among all tap locations at each wind direction, $\check{C}_P$. Comparisons of $\check{C}_P$ were made for the Sq-180°Hel & Corner cut, Sq-Tapered & 180°Hel, Sq-Tapered & 360° Hel & Corner cut, and Sq-Setback & 45° Rotate with Square, Sq-Tapered and Sq-Setback models to determine the combined effect of twisting and corner cut. The combined effects of corner cut & helical on $\check{C}_P$ are shown clearly in Figure 25. The magnitude of the negative peak pressure coefficients of the Sq-180°Hel & Corner cut model reduces for almost all wind directions other than for the Square model, whereas the combined effect of taper and helical on $\check{C}_P$ increases to higher magnitudes for the Sq-Tapered & 180°Hel model than for the Sq-Tapered model, as shown in Figure 26. The combined effect of taper, helical and corner cut (Sq-Tapered & 360°Hel & Corner cut model) shows slightly higher $\check{C}_P$ for some wind directions, and at the

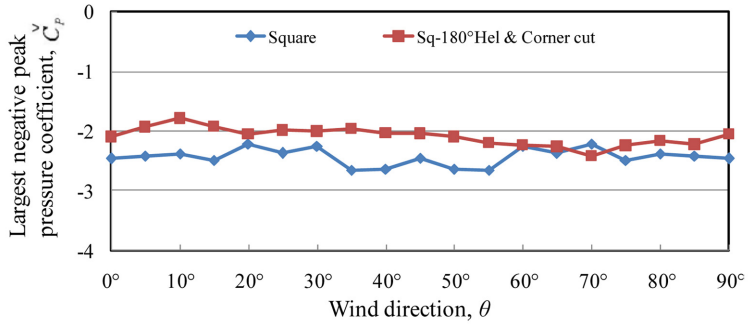


Figure 25. Variation of largest negative peak pressure coefficients with wind direction (θ) for Square and Sq-180°Hel & Corner cut model.

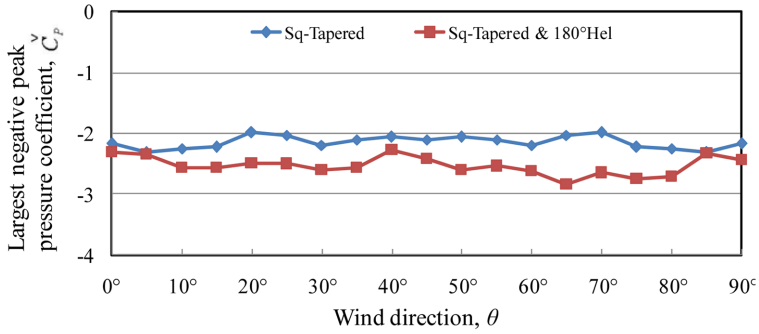


Figure 26. Variation of largest negative peak pressure coefficients with wind direction (θ) for the Sq-Tapered and Sq-Tapered & 180°Hel model.

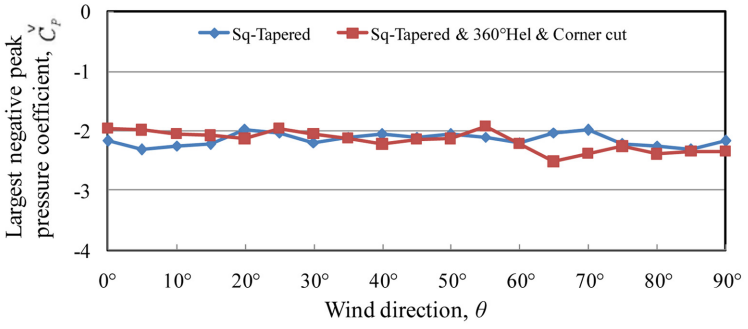


Figure 27. Variation of largest negative peak pressure coefficients with wind direction (θ) for the Sq-Tapered and Sq-Tapered & 360°Hel & Corner cut model.

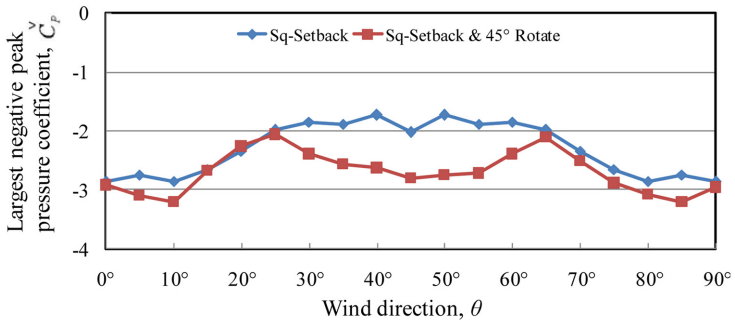
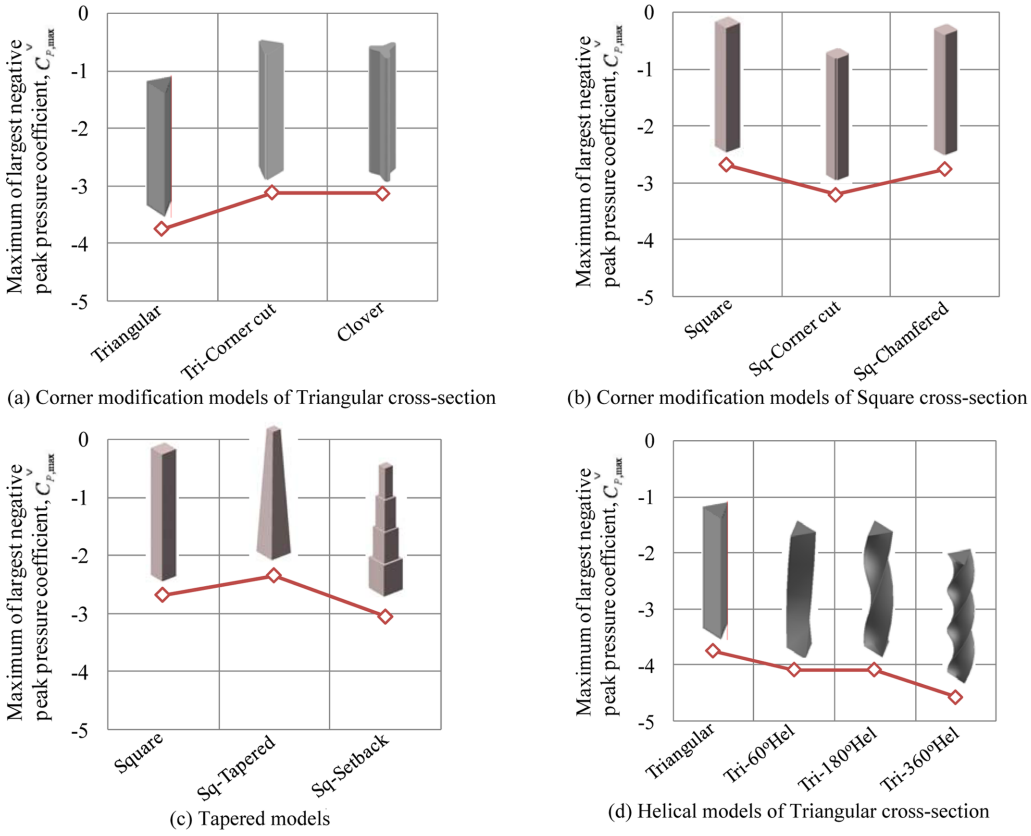


Figure 28. Variation of largest negative peak pressure coefficients with wind direction (θ) for the Sq-Setback and Sq-Setback & 45°Rotate.

same time lower values of $\check{C}_P$ occur for the Sq-Tapered model, as shown in Figure 27. The Sq-Setback & 45°Rotate model shows higher $\check{C}_P$ values than the Sq-Setback model for all wind directions, as shown in Figure 28.

3.6. Comparison of maximum largest negative peak pressure coefficients ($\check{C}_{p,\,max}$)

The maximum of the largest negative peak pressure coefficients ($\check{C}_{p,\,max}$) is the maximum value of $\check{C}_P$ among those for all the wind directions selected for each model. Figure 29(a)~(g) compares of $\check{C}_{p,\,max}$ for each category of models shown in Table 1. Due to the modification of corner regions, $\check{C}_{p,\,max}$ reduces and the values are equal for the Tri-Corner cut and Clover models. The $\check{C}_{p,\,max}$ value of the Sq-Corner cut model and the Sq-Setback model increases to around 16% and 12% greater than that of the Square model, as can be seen in Figure 29(b)~(c). For the Straight Polygonal models, the overall trend of $\check{C}_{p,\,max}$ decreases from Triangular model to Circular model, but the location of pressure tap may cause the slight variation in the trend for the Pentagon and Dodecagon models. As the twisting angle of the helical model increases, $\check{C}_{p,\,max}$ also increases for the Triangular and Square models, as can be seen in Figure 29(d). The polygonal helical models also show the same trend as the Straight Polygonal models, as can be seen in Figure 29(g). The combined effects of helical and corner cut



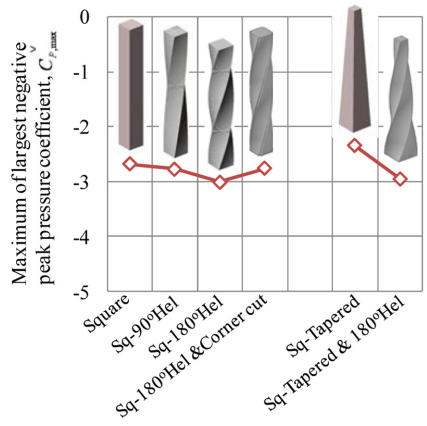
(a) Corner modification models of Triangular cross-section

(b) Corner modification models of Square cross-section

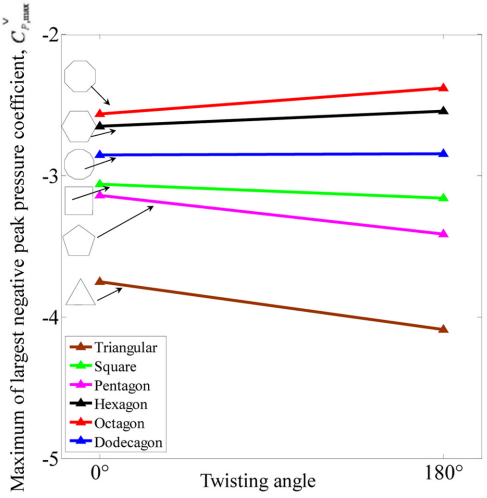
(c) Tapered models

(d) Helical models of Triangular cross-section

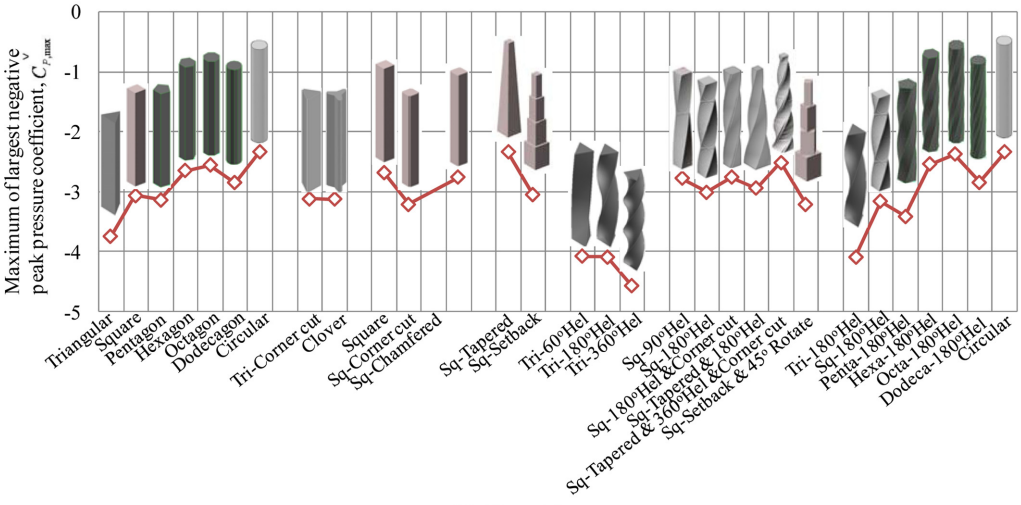
Figure 29. Comparison of maximum largest negative peak pressures ($\check{C}_{p,\,max}$).



(e) Helical models of Square cross-section



(f) Straight and 180°Helical models



(g) All models

Figure 29. Comparison of maximum largest negative peak pressures ($\check{C}_{p,\,max}$) (Continued).

(Sq-180°Hel & Corner cut model) decreases $\check{C}_{p,\,max}$ to 3% smaller than that of the Square model. The combined effect of tapering & helical (Sq-Tapered &180°Hel model) and helical & corner cut (Sq-Tapered & 360°Hel & Corner cut model) increases $\check{C}_{p,\,max}$ to around 20% and 7% greater than that of the Sq-Tapered model. The Sq-Setback model with 45°Rotation increases of $\check{C}_{p,\,max}$ to 5% greater than that of the Sq-Setback model value.

4. Conclusions

This paper has summarized the peak pressures on tall buildings of straight polygonal, tapered, helical, corner modification and combination models with various cross-sections under urban flow conditions. Based on the experimental results, the following conclusions are made.

(1) The largest negative peak ($\check{C}_p(i)$) occurs at the corner cut portion for both Tri-Corner cut and Sq-Corner cut models at 0.85*H*. The maximum largest negative peak pressure coefficient ($\check{C}_{p,\,max}$) for the Tri-Corner cut model is less than that for the Triangular model whereas for the Sq-Corner cut model is greater than that for the square model.

(2) The distribution of $\hat{C}_p(i)$ is smooth for all the straight models whereas for the Sq-Setback model it varies widely and the peak suctions occur at all the corners of each setback step, and $\check{C}_{p,\,max}$ of the Square model is around 88% that of the Sq-Setback model.

(3) For helical models, the distribution of $\check{C}_p(i)$ varies widely and peak suctions occur at the corners and even on the mid surfaces, but the area occupied by the peak suctions is very small for the helical models. When the twisting angle of the helical model increases, $\check{C}_p(i)$ and the height at which it occurs also increases for both Triangular (Tri-60°Hel, Tri-180°Hel and Tri-360°Hel) and square cross-sectional models (Sq-90°Hel and Sq-180°Hel). The variation of $\check{C}_p(i)$ between upper and lower levels decreases as the number of surfaces increases for the polygonal helical models.

(4) The overall trend of $\check{C}_{p,\,max}$ is reducing from Triangular model to Circular model. When the number of surfaces increases (polygonal models), $\check{C}_{p,\,max}$ decreases, whereas for the polygonal helical models, the trend of $\check{C}_{p,\,max}$ is the same as those for the polygonal models.

(5) Among all the combination models, the helical and corner cut combination shows much reduction in $\check{C}_{p,\,max}$ than that for the Square model.

(6) Among all the combination models, the Setback & 45°Rotate model has the highest value of $\check{C}_{p,\,max}$, but the distribution of $\check{C}_p(i)$ looks the same as that of the Sq-Setback model. $\check{C}_{p,\,max}$ for the Setback model is just 5% less than that of the Setback & 45°Rotate model.

Acknowledgements

This study was funded by the Strategic Japanese-Chinese Cooperative Program on "Science and Technology (S&T) for Environmental Conservation and Construction of a Society with Less Environmental Burden" (NSFC-JST) entitled "New Strategies for Wind Disaster Risk Reduction of Wind Sensitive Infrastructures" and Global Center of Excellence (Global COE), which is gratefully acknowledged.

References

Jamieson, N. J., Carpenter, P. and Cenek, P. D. (1992). "Wind induced external pressures on a tall building with various corner configurations." *Journal of Wind Engineering and Industrial Aerodynamics*, 41-44, pp. 2401~2412.

Katagiri Junji. (1992). Wind pressure characteristics of rectangular cylinders with cut corner, Summaries of technical papers of Annual Meeting, AIJ, 47-48. (in Japanese)

Ohtake Kazuo. (2000). Peak pressure coefficients for cladding of a tall building, Summaries of technical papers of Annual Meeting, AIJ, 193-194. (in Japanese)

Kikuchi Hirotoshi. (1997). Characteristics of peak wind pressures acting on a tall building model, Summaries of technical papers of Annual Meeting, AIJ, 209-210. (in Japanese)

Kim, Y. C. and Kanda, J. (2010). "Characteristics of aerodynamic force and pressures on square plan buildings with height variations." *Journal of Wind Engineering and Industrial Aerodynamics*, 98, pp. 449~465.

Melbourne, W. H. (1993). "Turbulence and the leading edge phenomenon." *Journal of Wind Engineering and Industrial Aerodynamics*, 49, pp. 45~64.

Ohtake Kazuo. (2000). Peak pressure coefficients for cladding of a tall building, Summaries of technical papers of Annual Meeting, AIJ, 193-194.

Saathoff, P. J. and Melbourne, W. H. (1989). "The generation of peak pressures in separated/reattaching flows." *Journal of Wind Engineering and Industrial Aerodynamics*, 32, pp. 121~134.

Stathopoulos, T. and Saathoff, P. (1991). "Wind pressure on roofs of various geometries." *Journal of Wind Engineering and Industrial Aerodynamics*, 38, pp. 273~284.

Surry, D. and Djakovich, D. (1995). "Fluctuating pressures on models of tall buildings." *Journal of Wind Engineering and Industrial Aerodynamics*, 58, pp. 81~112.